The role of hydrometeor fall speed in the scaling of precipitation extremes with temperature

Martin S. Singh[1] & Paul A. O'Gorman[1]

Simulations of radiative-convective equilibrium with a cloud-system resolving model are used to investigate the scaling of high percentiles of the precipitation distribution (precipitation extremes) over a wide range of surface temperatures. At surface temperatures characteristic of Earth's tropics or higher, precipitation extremes increase with warming in proportion to the increase in surface moisture, following what is termed Clausius-Clapeyron (CC) scaling. At lower temperatures, the rate of increase of precipitation extremes depends on the period of accumulation considered and exceeds CC scaling for accumulation periods of one hour or less. The reason for this higher rate of increase is found to be a change in the mean fall speed of hydrometeors that accompanies changes in the relative proportions of snow and rain in the column. The possible relevance of these results to recent observations of high rates of increase of precipitation extremes with temperature is discussed.

1. Introduction

Increases in the intensity of precipitation extremes are seen in simulations of climate warming [*Kharin et al.*, 2007; *O'Gorman and Schneider*, 2009] and have been identified in observational trends [*Westra et al.*, 2013]. Analyses of variability in the current climate also show a relation between precipitation extremes and the temperature at which they occur [e.g., *Allan and Soden*, 2008; *Lenderink and van Meijgaard*, 2008]. However, the rate at which precipitation extremes strengthen as the climate warms remains uncertain to the extent that they involve moist-convective processes that are difficult to represent in climate models [*Wilcox and Donner*, 2007; *O'Gorman*, 2012].

Here we investigate the precipitation distribution in simulations with a cloud-system resolving model (CRM) in the idealized setting of radiative-convective equilibrium (RCE). Previous studies of the precipitation distribution in RCE have found that, at surface temperatures characteristic of Earth's tropics, precipitation extremes increase with warming following what is known as Clausius-Clapeyron (CC) scaling, increasing roughly in proportion to the saturation specific humidity near the surface [*Muller et al.*, 2011; *Romps*, 2011]. This conclusion holds even when the convection is organized [*Muller*, 2013]. CC scaling of precipitation extremes with surface temperature is consistent with a simple view of the response of strong precipitation events to warming in which the amount of converged water vapor increases due to the increased amount of moisture near the surface. However, the close agreement with CC scaling found in modeling studies of RCE may be coincidental because the water-vapor convergence does not occur only at the surface and the strength and vertical profile of the updraft changes with warming [*Muller et al.*, 2011; *Romps*, 2011]. In this study, we extend previous results to a wider range of surface temperatures and find that, in general, precipitation extremes in RCE do not follow a simple scaling based on the amount of near-surface moisture. In particular, for accumulation periods shorter than one hour and surface temperatures lower than 295 K, precipitation extremes increase with warming at a considerably higher rate than implied by CC scaling.

We argue that the high rate of increase of precipitation extremes found in our simulations is a result of a change in the mean fall speed of hydrometeors in a warming atmosphere. In simulations in which the fall speeds of hydrometeors are fixed to a constant value, the increase of precipitation extremes with warming is generally at a lower rate than predicted by CC scaling, and the precipitation extremes depend strongly on the imposed fall speed. When interactive fall speeds are included, the mean fall speed of precipitation increases with temperature as the makeup of hydrometeors in the column switches from being dominated by slowly falling snow to more rapidly falling rain. The rate of increase of precipitation extremes may then be seen to be largely a result of the increase in surface moisture in combination with the increase in hydrometeor fall speed as the atmosphere warms. A role for hydrometeor fall speeds in determining both the precipitation intensity and the updraft strength in RCE has been suggested previously [*Parodi and Emanuel*, 2009; *Parodi et al.*, 2011]. Here we find that the hydrometeor fall speed affects the precipitation rate through changes in precipitation efficiency, but that the effect on updrafts is weak.

While the results we will show are for the idealized case of RCE, the mechanisms involved are sufficiently general to be of potential relevance to Earth's atmosphere. Observational relationships between temperature and precipitation extremes on sub-daily timescales can vary substantially by region [*Hardwick Jones et al.*, 2010], but analyses of station observations have suggested a scaling of precipitation extremes with temperature of up to twice the CC rate at particular locations [*Lenderink and van Meijgaard*, 2008; *Lenderink et al.*, 2011; *Berg et al.*, 2013]. The increase in the fall speed of hydrometeors accompanying warming is one possible mechanism contributing to such high rates of increase of precipitation extremes.

2. Precipitation extremes in radiative-convective equiilbrium

We investigate precipitation extremes in a series of simulations of RCE conducted using version 16 of the Bryan Cloud Model [*Bryan and Fritsch*, 2002]. These simulations are similar to those described in *Singh and O'Gorman* [2013] where the focus was on understanding increases in convective available potential energy in RCE with warming. The model is compressible and non-hydrostatic, and

[1]Department of Earth, Atmospheric & Planetary Sciences, Massachusetts Institute of Technology, Cambridge, Massachusetts, USA.

0094-8276/14/$5.00

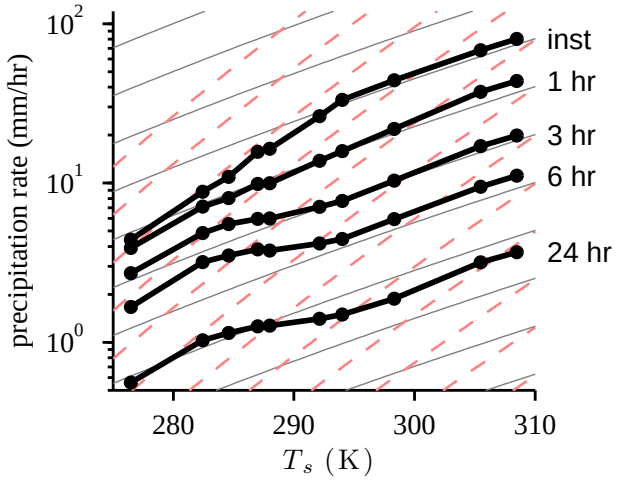

Figure 1. 99.99th percentile of precipitation rate in high-resolution simulations (black lines) calculated using various accumulation periods and shown as a function of the mean temperature at the lowest model level (T_s). Accumulation periods of one model time-step (inst), one hour (1 hr), three hours (3 hr), six hours (6 hr) and one day (24 hr) are shown. Gray lines are contours proportional to the surface saturation specific humidity, and red-dashed lines are contours proportional to the square of the surface saturation specific humidity; each successive line corresponds to a factor of two increase.

uses 6th order spatial differencing coupled with a 6th order diffusion scheme for numerical stability, and a split time-stepping scheme following *Wicker and Skamarock* [2002]. Bulk aerodynamic formulae are used to calculate the surface fluxes, with exchange coefficients determined based on Monin-Obukov similarity theory. Sub-grid scale motions are parameterized through a Smagorinsky turbulence scheme with different diffusion coefficients in the horizontal and vertical [*Bryan and Rotunno*, 2009]. The simulations include a band-averaged radiative transfer scheme, but no diurnal cycle; all simulations are performed with a constant solar flux of 390 W m^{-2} incident at a zenith angle of 43°. Microphysics are treated using a six-species, one-moment scheme based on *Lin et al.* [1983] in which there are three hydrometeor species (rain, snow and hail) each with a different fall speed that depends on mixing ratio.

We present results based on a series of simulations in which each simulation has a different imposed CO_2 concentration in the range 1 – 640 ppmv. The series is run at three different horizontal resolutions, with all simulations including 64 vertical levels. First, a set of low-resolution simulations (2 km horizontal grid-spacing, 80 × 80 km domain) are run to equilibrium over a slab ocean of depth 1 m. These slab-ocean simulations achieve equilibrium SSTs in the range 281 – 311 K. A set of intermediate-resolution simulations (1 km horizontal grid spacing, 84 × 84 km domain) and a set of high-resolution simulations (0.5 km horizontal grid spacing, 160 × 160 km domain) are then conducted with the same range of CO_2 concentrations and using the equilibrium SSTs of the corresponding slab-ocean simulations as a fixed lower boundary condition. The intermediate-resolution simulations are each run for 40 days, and the high-resolution simulations are run for 30 days. In both cases we begin collecting statistics at hourly intervals after 20 days of simulation. Results are broadly similar across resolutions; we show results from the high resolution simulations in this section, but in following sections we switch to the intermediate-resolution results to allow direct comparison with additional intermediate-resolution simulations in which the fall speeds of hydrometeors are set to fixed values.

Fig. 1 shows precipitation extremes as measured by the 99.99th percentile of gridbox precipitation rates (zero precipitation rates are included when calculating percentiles) in the high-resolution simulations as a function of the mean temperature in the lowest model level (T_s) and for different accumulation time periods. The precipitation extremes increase as the accumulation period decreases, with the highest values occurring for instantaneous (i.e., accumulated over one model time step) precipitation extremes. The fractional rate of increase of precipitation extremes with warming also varies with the accumulation period used. At surface temperatures below $\sim$ 295 K instantaneous precipitation extremes increase rapidly with temperature, exceeding the rate of increase given by CC scaling (gray lines) of 6-7% K^{-1} and approaching twice that rate (red-dashed lines). As the surface temperature increases above 295 K the rate of increase drops to be very close to that implied by CC scaling.

At longer accumulation periods of 3 hours and above, precipitation extremes increase at a rate that is generally close to that implied by CC scaling, although there is some variability in the rate of increase with temperature. At an intermediate accumulation period of one hour the rate of increase of precipitation extremes is somewhat higher than CC scaling at most temperatures. Consistent with previous studies [*Muller et al.*, 2011; *Romps*, 2011], the rate of increase of precipitation extremes at surface temperatures typical of Earth's tropics is close to that implied by CC scaling at all accumulation periods.

The scaling of precipitation extremes documented here is somewhat sensitive to the percentile chosen. Higher percentiles (99.999th) show results consistent with Fig. 1, but lower percentiles (99.9th) show considerable variation in the rate of increase of precipitation extremes with warming. Nevertheless, instantaneous precipitation extremes generally increase at a rate substantially higher than implied by CC scaling over part of the range of temperatures simulated. This super-CC increase is worthy of further investigation since similar rates of increase have been reported in sub-daily station observations at both sub-tropical and temperate latitudes when precipitation is binned by daily mean surface temperature [*Lenderink and van Meijgaard*, 2008; *Lenderink et al.*, 2011].

3. Scaling of condensation extremes with surface temperature

To examine the processes leading to deviations in the rate of increase of precipitation extremes from CC scaling we first consider extremes of the column net-condensation rate (Fig. 2a). The column net-condensation rate refers to the instantaneous condensation rate minus the instantaneous evaporation rate integrated over a column. Net-condensation extremes increase at a rate close to or slightly less than the CC rate over all temperatures, in contrast to the super-CC increase in instantaneous precipitation extremes, and despite the peak vertical velocity conditioned on net-condensation extremes increasing from 7 to 12 m s^{-1} over the range of temperatures simulated (Fig. 3). In order to explain the sub-CC scaling of net-condensation extremes in light of the increase in peak updraft strength we consider a decomposition of the net condensation similar to that given by *Muller et al.* [2011]:

$$C_e = \epsilon_C \int_0^{z_t} \frac{\partial \overline{q^*}}{\partial z} \overline{\rho} w_e \, dz. \qquad (1)$$

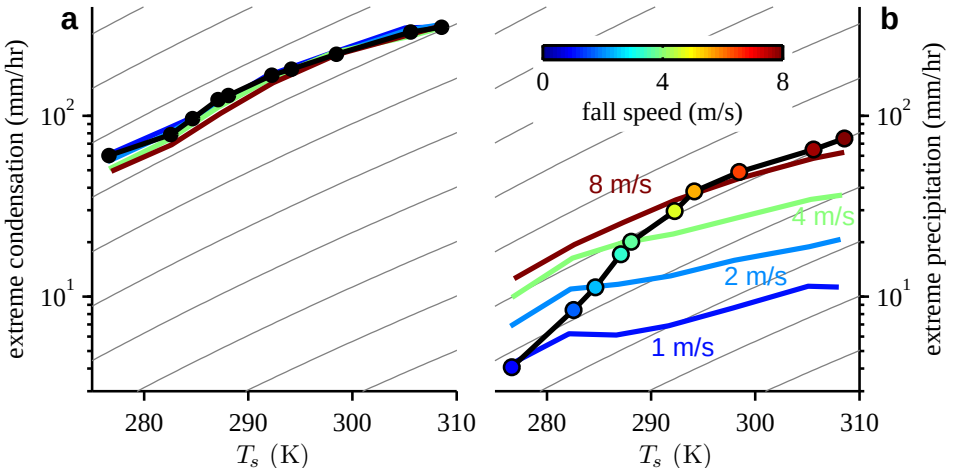

Figure 2. The 99.99th percentile of instantaneous (a) column net-condensation rate and (b) surface precipitation rate as a function of the mean temperature of the lowest model level (T_s) in intermediate-resolution simulations. Black lines correspond to full-microphysics simulations while colored lines show results from simulations in which the fall speed of all hydrometeors is set to constant values of 1 (blue), 2 (cyan), 4 (green) and 8 (maroon) m s^{-1}. Marker colors in (b) correspond to the effective fall speed of hydrometeors in the full-microphysics simulations (see text). Thin gray lines are contours proportional to the surface saturation specific humidity, with each successive line corresponding to a factor of two increase.

Here C_e is the 99.99th percentile of column net condensation, ρ is the density, q^* is the saturation specific humidity, the over-bar represents a time and domain mean and z_t is the height of the tropopause. The vertical velocity profile w_e is calculated as the mean vertical velocity for points in which the column net-condensation rate exceeds its 99.99th percentile. The integral in (1) represents an estimate of the column net-condensation rate derived from the dry static energy budget [see *Muller et al.*, 2011]. The inaccuracies in the estimate associated with the approximations made in the derivation are collected into the condensation efficiency ϵ_C so that (1) is exactly satisfied.

Consider the simple case in which the mass flux $\overline{\rho} w_e$ during net-condensation extremes is constant in the vertical except for near the surface, where there is strong convergence, and near the tropopause, where there is strong divergence. The integral in (1) may then be approximately evaluated as proportional to the near-surface saturation specific humidity [*O'Gorman and Schneider*, 2009; *Muller et al.*, 2011]. If we further assume there are no changes in the mass flux or condensation efficiency with warming, condensation extremes must increase with warming at the CC rate.

Deviations of net-condensation extremes from CC scaling result from a more realistic mass-flux profile, or from changes in the mass-flux profile or efficiency ϵ_C with temperature. In particular, the expression for the condensation rate (1) includes the vertical velocity within an integral weighted by the vertical gradient in saturation specific humidity. This vertical gradient maximizes at the surface and decreases exponentially above, making the low-level vertical velocity critical in setting the net-condensation rate. In our simulations, w_e decreases with warming at levels below 800 hPa. Low-level changes in w_e, therefore, have a negative influence on net-condensation extremes, explaining how the peak updraft increases but the net-condensation rate increases at a rate lower than that implied by CC scaling. We find that the condensation efficiency ϵ_C decreases between 0.84 and 0.74 across the intermediate-resolution simulations (not shown), also contributing to the sub-CC scaling of instantaneous net condensation in the simulations.

4. The effect of the fall speed of hydrometeors on precipitation extremes

It is useful to represent the relationship between instantaneous net-condensation extremes and instantaneous precipitation extremes by an efficiency ϵ_P such that,

$$P_e = \epsilon_P C_e, \tag{2}$$

where P_e is the 99.99th percentile of the precipitation rate. Since we consider net-condensation, and since the occurrence of precipitation extremes may not be exactly col-

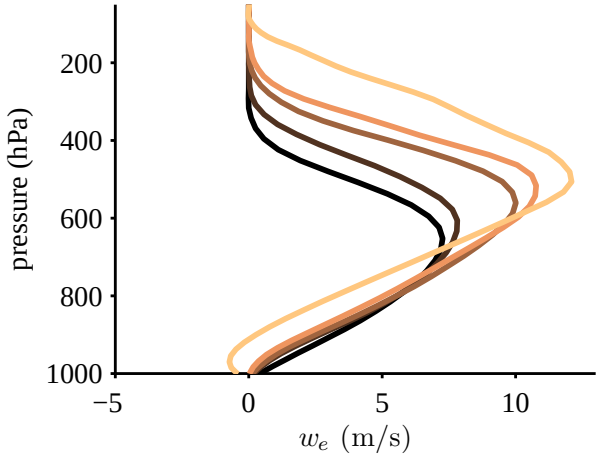

Figure 3. Mean vertical velocity profiles for points in which the instantaneous net-condensation rate in the column exceeds its 99.99th percentile. Intermediate-resolution simulations with mean temperatures of the lowest model level (T_s) of 277 (black), 285, 292, 298 and 309 K (orange) are shown.

located in space and time with the occurrence of net-condensation extremes, ϵ_P is not a precipitation efficiency in the traditional sense. Nevertheless, ϵ_P represents the efficiency by which large net-condensation events are translated into large precipitation events as the condensate falls to the surface.

At low temperatures, the fractional rate of increase of instantaneous precipitation extremes with warming is larger than that of instantaneous net-condensation extremes, indicating that ϵ_P increases with warming. The value of ϵ_P is determined by the degree to which the precipitation is spread out relative to the column net-condensation both spatially and temporally, as well as the fraction of condensation that evaporates in the time between the net-condensation event and its related precipitation event. These mechanisms are particularly sensitive to the microphysical properties of clouds. For instance, in the limit of instantaneous removal of condensate from the atmosphere, the precipitation rate equals the condensation rate, and ϵ_P is unity at all temperatures. In the opposite limit, in which condensed water takes a long time to form precipitation or the hydrometeor fall speed is low, turbulence and the cloud-scale circulation have a long time to act in removing the condensate from the column, and the precipitating hydrometeors may spend long periods of time in sub-saturated air (Fig. 4a). A low hydrometeor fall speed may also affect ϵ_P by spreading out the precipitation in time. Since the condensation occurs at a range of heights, precipitation will reach the ground at different times, even if the condensation were to occur at a single instant. If the timescale over which precipitation falls out is larger than the timescale of condensation events, this has the effect of spreading the precipitation event over a longer time period relative to the condensation event (Fig. 4b). For instantaneous precipitation extremes a lower hydrometeor fall speed would tend to reduce ϵ_P, but for precipitation accumulation times substantially longer than an individual convective event ($\sim$ 1 hour) the effect would be minimal.

The hydrometeor fall speed is sensitive to temperature changes; snow has typical fall speeds of 0.5 – 1 m s^{-1}, while rain often falls at speeds of 5 – 8 m s^{-1}. In the coldest simulations, precipitating hydrometeors spend most of their life as snow even though the surface precipitation is almost entirely in liquid form. We hypothesize that the super-CC scaling of precipitation extremes seen in the simulations is a result of a transition in hydrometeor distribution from a snow dominated regime to a rain dominated regime.

To investigate this hypothesis we examine additional intermediate-resolution simulations in which the model microphysics are altered such that the fall speed of all hydrometeors are fixed to a constant value. Sets of simulations are conducted with fall speeds in the range 1 – 8 m s^{-1}; for each fall speed, seven simulations are run with different SST boundary conditions corresponding to a subset of the SSTs used in the full-microphysics simulations described in section 2. Apart from the values of the fall speeds of snow, rain and hail, the model used for each of these simulations is identical to the model used for the corresponding full-microphysics simulation at the same SST.

Previous work has shown that the hydrometeor fall speed strongly affects precipitation rates in RCE [*Parodi et al.*, 2011]. *Parodi and Emanuel* [2009] also showed that the fall speed influenced updraft velocities in moist convection. But in the simulations shown here net-condensation extremes (Fig. 2a) and the magnitude of the strongest updrafts (not shown) are relatively insensitive to the hydrometeor fall speed. Some dependence of the updraft strength on hydrometeor fall speed is found if only warm-rain microphysical processes are allowed as in *Parodi and Emanuel* [2009], but in general the effect of hydrometer fall speed

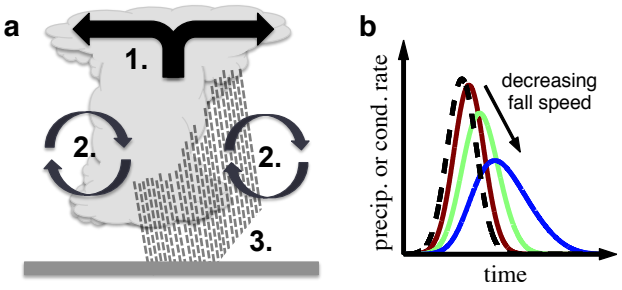

Figure 4. Schematic showing mechanisms affecting the value of ϵ_P. (a) Removal of liquid and solid water from the column by (1) the cloud-scale circulation and (2) turbulence (both resolved and sub-grid), as well as (3) evaporation and sublimation of precipitation. (b) Spreading of the precipitation event in time as the hydrometeor fall speed decreases (maroon to green to blue). Dashed black line represents the column net-condensation rate.

on ϵ_P is a much larger factor in determining the intensity of precipitation extremes. An increase in fall speed from 1 to 8 m s^{-1} results in an increase in instantaneous precipitation extremes by more than a factor of five at a surface temperature of T_s = 298 K (Fig. 2b). (For the case of 3 hourly accumulation this factor is reduced to approximately 2.5.) On the other hand, increasing the surface temperature while keeping the hydrometeor fall speed fixed results in an increase in precipitation extremes somewhat less than predicted by CC scaling.

An effective hydrometeor fall speed is defined by taking the hydrometeor-mass weighted mean of the fall speeds of all hydrometeors in the column conditioned on the precipitation rate exceeding its 99.99th percentile. In the fixed fall-speed simulations this is simply equal to the imposed hydrometeor fall speed. In the simulations with full microphysics, the effective fall speed ranges from less than 1 m s^{-1} in the coldest simulation to above 7 m s^{-1} in the warmest simulation (Fig. 2b). This is primarily a result of the increasing fraction of rain compared to snow in the column as the atmosphere warms, but the increase in rain mixing ratios with warming also increases the mean fall speed of rain itself. Hail has a fall speed larger than both snow and rain, but it contributes only a small fraction of the total hydrometeor loading of the atmosphere.

The precipitation extremes in a given full-microphysics simulation are roughly consistent with those in a fixed fall-speed simulation at the same surface temperature and with the same effective fall speed (compare the marker colors and line colors in Fig. 2b). This implies that without the change in fall speed, the increase of precipitation extremes with warming in the full-microphysics simulations would be somewhat below the CC rate. We thus conclude that the super-CC increase in instantaneous precipitation extremes found in the full-microphysics simulations is a result of the increase in the mean fall speed of hydrometeors that accompanies a switch from a snow-dominated to a rain-dominated hydrometeor distribution. Even for longer accumulation periods, the increase in precipitation extremes with warming for simulations with fixed hydrometeor fall speeds is less than the CC rate (not shown). The rough CC-scaling of precipitation extremes at accumulation periods longer than one hour in the full-microphysics simulations appears to result from increases in hydrometeor fall speed that increase the precipitation efficiency relative to the fixed fall-speed case.

5. Conclusions

We have investigated the relationship between precipitation extremes and surface temperature in CRM simulations of RCE. At temperatures characteristic of Earth's tropics or higher, the increase in precipitation extremes with warming is consistent with Clausius-Clapeyron scaling, whereby precipitation extremes scale with the near-surface saturation specific humidity. At lower surface temperatures the rate of increase of precipitation extremes with warming depends on the accumulation period under consideration. For accumulation periods of one hour or less stronger increases in precipitation extremes than expected from CC scaling are found over a broad range of temperatures, and at the shortest timescale the increase in precipitation extremes with warming approaches twice the CC rate. For longer accumulation periods, the rate of increase in precipitation extremes depends somewhat on temperature, but remains relatively close to the CC rate.

The reasons for the super-CC scaling of precipitation extremes are found to relate to changes in the fall speed of hydrometeors as the surface temperature is increased. At low temperatures, the precipitating water in the column is primarily composed of snow, while at higher temperatures it is primarily composed of rain, which falls at much faster speeds. The fall speed of hydrometeors has a large impact on precipitation rates in the simulations, consistent with recent studies [*Parodi and Emanuel*, 2009; *Parodi et al.*, 2011]. But unlike *Parodi and Emanuel* [2009], the updraft velocity is relatively insensitive to changes in hydrometeor fall speed. The effect of hydrometeor fall speed on precipitation extremes in the simulations shown here is a result of changes in the efficiency with which large net-condensation events are translated into large precipitation events. The changing efficiency is likely to be a result of a changing fraction of condensate that is turbulently diffused out of the column or re-evaporated before reaching the ground, as well as, for short accumulation periods, a spreading out of the precipitation event in time. In simulations in which the model microphysics are altered such that hydrometeors fall at a fixed speed, precipitation extremes increase with temperature more slowly than the CC rate. These results suggest that, absent changes in fall speed, the rate of change of precipitation extremes with warming would not necessarily be close to the CC rate, even for accumulation periods longer than one hour.

The increase of hydrometeor fall speed with temperature across the simulations is qualitatively consistent with a shift from snow to rain and is likely to be a robust result because of the large difference in the fall speeds of snow and rain. Snow falls relatively slowly (~ 0.6 m s^{-1}) in the particular implementation of the one-moment microphysical parameterization of *Lin et al.* [1983] used in the simulations for this study. Additional simulations in which the hydrometeor fall speeds are calculated identically to *Lin et al.* [1983] as updated by *Potter* [1991] have slightly faster falling snow but show similar results for the scaling of precipitation extremes.

The super-CC scaling of precipitation extremes with temperature seen in the simulations resembles the scaling of precipitation extremes found in some high temporal-resolution station observations when stratified by surface temperature [*Berg et al.*, 2013]. It has been argued that this observed super-CC scaling of precipitation extremes is the result of stronger updrafts occuring during warm events [*Loriaux et al.*, 2013]. In the simulations shown here, changes in updraft velocity only weakly affect the precipitation rate, and it is the fall speed of hydrometeors that is important for the scaling of precipitation extremes. One discrepancy is that the observed super-CC scaling of precipitation extremes with temperature occurs for accumulation periods of both one hour and 5 minutes [*Berg et al.*, 2013], while in the simulations the instantaneous precipitation extremes exceed CC scaling to a greater extent than the hourly precipitation extremes. Additionally, other high-resolution precipitation observations do not show robust scaling of precipitation extremes at greater than the CC rate in response to local temperature variation [*Hardwick Jones et al.*, 2010]. Further study is required to evaluate under what conditions the mechanisms outlined here in simulations of RCE may be relevant for convective precipitation in the mid-latitudes and sub-tropics in the current climate or under climate change.

Acknowledgments. Model results were obtained using the numerical code CM1, maintained by G. Bryan and available at http://www.mmm.ucar.edu/people/bryan/cm1/. High-performance computing support from Yellowstone (ark:/85065/d7wd3xhc) was provided by NCAR's Computational and Information Systems Laboratory, sponsored by the NSF. We acknowledge support from NSF grant AGS-1148594 and NASA ROSES grant 09-IDS09-0049.

References

Allan, R. P., and B. J. Soden (2008), Atmospheric warming and the amplification of precipitation extremes, *Science*, *321*, 1481–1484.

Berg, P., C. Moseley, and J. O. Haerter (2013), Strong increase in convective precipitation in response to higher temperatures, *Nat. Geosci.*, *6*, 181–185.

Bryan, G. H., and J. M. Fritsch (2002), A benchmark simulation for moist nonhydrostatic numerical models, *Mon. Wea. Rev.*, *130*, 2917–2928.

Bryan, G. H., and R. Rotunno (2009), The maximum intensity of tropical cyclones in axisymmetric numerical model simulations, *Mon. Wea. Rev.*, *137*, 1770–1789.

Hardwick Jones, R., S. Westra, and A. Sharma (2010), Observed relationships between extreme sub-daily precipitation, surface temperature, and relative humidity, *Geophys. Res. Lett.*, *37*, L22,805, doi:10.1029/2010GL045081.

Kharin, V. V., F. W. Zwiers, X. Zhang, and G. C. Hegerl (2007), Changes in temperature and precipitation extremes in the IPCC ensemble of global coupled model simulations, *J. Climate*, *20*, 1419–1444.

Lenderink, G., and E. van Meijgaard (2008), Increase in hourly precipitation extremes beyond expectations from temperature changes, *Nature Geosci.*, *1*, 511–514.

Lenderink, G., H. Y. Mok, T. C. Lee, and G. J. van Oldenborgh (2011), Scaling and trends of hourly precipitation extremes in two different climate zones – Hong Kong and the Netherlands, *Hydrol. Earth Syst. Sci.*, *15*, 3033–3041.

Lin, Y.-L., R. D. Farley, and H. D. Orville (1983), Bulk parameterization of the snow field in a cloud model, *J. Clim. Appl. Meteorol.*, *22*, 1065–1092.

Loriaux, J. M., G. Lenderink, S. R. De Roode, and A. P. Siebesma (2013), Understanding convective extreme precipitation scaling using observations and an entraining plume model, *J. Atmos. Sci*, *70*, 3641–3655.

Muller, C. (2013), Impact of convective organization on the response of tropical precipitation extremes to warming, *J. Climate*, *26*, 5028–5043.

Muller, C. J., P. A. O'Gorman, and L. E. Back (2011), Intensification of precipitation extremes with warming in a cloud-resolving model, *J. Climate*, *24*, 2784–2800.

O'Gorman, P. A. (2012), Sensitivity of tropical precipitation extremes to climate change, *Nature Geosci.*, *5*, 697–700.

O'Gorman, P. A., and T. Schneider (2009), The physical basis for increases in precipitation extremes in simulations of 21st-century climate change, *Proc. Nat. Acad. Sci.*, *106*, 14,773–14,777.

Parodi, A., and K. Emanuel (2009), A theory for buoyancy and velocity scales in deep moist convection, *J. Atmos. Sci.*, *66*, 3449–3463.

Parodi, A., E. Foufoula-Georgiou, and K. Emanuel (2011), Signature of microphysics on spatial rainfall statistics, *J. Geophys. Res.*, *116*, D14,119, doi:10.1029/2010JD015124.

Potter, B. E. (1991), Improvements to a commonly used cloud microphysical bulk parameterization, *J. Appl. Meteorol.*, *30*, 1040–1042.

Romps, D. M. (2011), Response of tropical precipitation to global warming, *J. Atmos. Sci.*, *68*, 123–138.

Singh, M. S., and P. A. O'Gorman (2013), Influence of entrainment on the thermal stratication in simulations of radiative-convective equilibrium, *Geophys. Res. Lett.*, *40*, 4398-4403, doi:10.1002/grl.50796.

Westra, S., L. V. Alexander, and F. W. Zwiers (2013), Global increasing trends in annual maximum daily precipitation, *J. Climate*, *26*, 3904–3918.

Wicker, L. J., and W. C. Skamarock (2002), Time-splitting methods for elastic models using forward time schemes, *Mon. Wea. Rev.*, *130*, 2088–2097.

Wilcox, E. M., and L. J. Donner (2007), The frequency of extreme rain events in satellite rain-rate estimates and an atmospheric general circulation model, *J. Climate*, *20*, 53 – 69.

Corresponding author: M.S. Singh, Department of Earth, Atmospheric and Planetary Sciences, Massachusetts Institute of Technology, 77 Massachusetts Ave., Cambridge, MA 02139, USA. (mssingh@mit.edu)